ELSEVIER

Thermochimica Acta 314 (1998) 87–110

thermochimica acta

Experimental investigation and thermodynamic calculation of the Al–Mg–Zn system

P. Liang[a,*], T. Tarfa[b], J.A. Robinson[c], S. Wagner[a], P. Ochin[b], M.G. Harmelin[b], H.J. Seifert[a], H.L. Lukas[a], F. Aldinger[a]

[a] *Max-Planck-Institut für Metallforschung, Pulvermetallurgisches Laboratorium, Heisenbergstr. 5, D-70569 Stuttgart, Germany*
[b] *Centre d'Etudes de Chimie Métallurgique, CNRS, 15 rue Georges Urbain, F-94407 Vitry-sur-Seine Cedex, France*
[c] *Materials Science Center, University of Manchester and UMIST, Manchester, UK*

Received 8 September 1997; accepted 14 October 1997

Abstract

On the basis of a critical assessment, experimental investigations by EPMA on ternary Al–Mg–Zn alloys were specifically performed to provide missing data of the ternary solubilities of the Al–Mg and Mg–Zn phases as well as to improve the knowledge of the extensions of the homogeneity ranges of the ternary τ- and Φ-phases. A thermodynamic description for the Al–Mg–Zn system was obtained taking into account those experimental data together with constitutional, thermodynamic and crystallographic literature information. The binary intermetallic phases are modelled to have ternary solubilities. The ternary τ-phase is modelled according to its crystal structure with cubic symmetry as $(Mg)_{26}$(**Mg**, Al)$_6$(**Al**, **Zn**, Mg)$_{48}$(Al)$_1$ in the compound-energy-formalism. The Φ-phase is described by the sublattice formula Mg_6(**Al**, **Zn**)$_5$. © 1998 Elsevier Science B.V.

Keywords: Al–Mg–Zn; Phase diagram; Thermodynamics; EPMA; DTA

1. Introduction

The quaternary system Al–Cu–Mg–Zn is one of the key systems of high strength Al alloys. The 7xxx-series alloys in which zinc, copper and magnesium are the major alloying elements, are the highest-strength aluminium-base alloys commercially available. They are extensively used in aircraft construction and other high-strength applications.

For successful development of new materials and improvement of existing Al alloys, the knowledge of phase diagrams and thermodynamic data is crucial. In the framework of the COST Action 507, which is concerned with the measurement and evaluation of thermochemical and thermophysical properties to provide a database for the development of new light metal alloys, the development of a thermodynamic description of the quaternary system Al–Cu–Mg–Zn is proposed. All the binary subsystems have been already evaluated in the COST-507 project [1]. The binary systems Al–Mg [2] and Mg–Zn [3] could be improved in the present study using new experimental results. Thermodynamic descriptions for the ternaries Al–Cu–Mg [4], Al–Mg–Zn [5] and Cu–Mg–Zn [5] as well as for the Al-rich corner of the ternary system Al–Cu–Zn [6], have been also developed in the COST-507 project.

*Corresponding author. Fax: 0049 7116861131; e-mail: liang@aldix.mpi-stuttgart.mpg.de

PII S0040-6031(97)00458-9

In this work we present experimental investigations and a thermodynamic description of the Al–Mg–Zn system. The phase equilibria of this ternary system are also of practical interest in the development of Al- and Mg-based alloys. For an accurate thermodynamic description, however, some specific experiments were desirable. In the present work, experimental investigations on Al–Mg–Zn alloys were specifically performed to provide missing data of the ternary solubilities of the Al–Mg and Mg–Zn phases as well as to improve the knowledge of the extensions of the homogeneity ranges of the ternary τ- and Φ-phases by X-ray diffraction (XRD), Differential Thermal Analysis (DTA), Differential Scanning Calorimetry (DSC), and Electron Probe MicroAnalysis (EPMA). The results of these experiments, together with literature data, were used to determine a complete set of thermodynamic descriptions of all stable phases of the Al–Mg–Zn system.

2. Literature review

The experimental phase diagram data and thermodynamic data in the literature are summarized in Table 1. The first summarizing review was done by Willey [7]. Later critical assessments of the experimental phase diagram and thermodynamic data are from Despande et al. [8] and Petrov [9].

In the Al–Mg–Zn system there exist eleven binary and two ternary solid phases. The crystallographic data are summarized in Table 2.

2.1. Phase diagram data

2.1.1. Intermetallic ternary compounds

The entire Al–Mg–Zn system was investigated for the first time by Eger [10] by means of thermal analysis and metallography. The author established the presence of a ternary phase, with a tentatively wide homogeneity range along the section from $MgZn_2$ to γ-Al–Mg. This phase is named τ in our paper. The structure of the τ-phase was first determined by Laves et al. [11] for a composition given as $Mg_3Zn_3Al_2$. Later the complete determination of the crystal structure was carried out by Bergman et al. [12,13] and an idealized formula $Mg_{32}(Al, Zn)_{49}$ was proposed (see Table 2). However, the extension of the homogeneity range of τ [14–21] show that there must be also Mg-occupation on Al, Zn sublattices as well as Al- or Zn-occupation on Mg sublattices.

The other ternary intermetallic phase, the Φ-phase, was discovered by Clark [21]. Its unit cell has been recently determined [22] (see Table 2). The solubility range of the Φ-phase is narrow along a composition line close to 53–55 at.% Mg, Al and Zn contents vary approximately from 18 to 29 and from 28 to 17 at.%, respectively [22].

Alloys with compositions in the area of τ and Φ have been reported to form icosahedral quasicrystals (with 5-fold symmetry) when quenched from liquid or when mechanically alloyed [23–25]. These quasicrystals are metastable and transform on annealing to the stable τ- and Φ-phases.

2.1.2. Liquidus surface

Eger [10] was the first to construct the liquidus surface for the entire composition range of Al–Mg–Zn. Other investigations [14–17,20,21,26–32] are listed in Table 1. Willey [7], in a brief but rather detailed review, gave a liquidus surface close to that proposed by Clark [21]. The liquidus surface of [7] has been adopted without changes by Despande et al. [8] and generally agrees with the data of the reviews by Mondolfo [33,34].

2.1.3. Invariant equilibria

Three reaction schemes can be found in the experimental literature devoted to the Al–Mg–Zn system. They relate to the Mg corner [17], the Mg corner of the system above the line 50 at.% Mg [21] and to the Zn corner [15], respectively. The ternary peritectic formation of the Φ-phase, $L+\gamma+\tau \rightleftharpoons \Phi$, was experimentally proved by Clark [21]. These authors also concluded that the liquidus surface must reach a minimum at a eutectic point, $L \rightleftharpoons (Mg)+MgZn+\tau$, as reported by Mikheeva and Kryukova [30]. However, literature research revealed there is uncertainty about the existence of some ternary invariant reactions: temperatures of the invariant reactions p_1 ($L+MgZn_2 \rightleftharpoons \tau$) and D ($L \rightleftharpoons (Al)+MgZn_2,\tau$) have been assessed as 535°C and 475°C respectively by Petrov [9], but different values were given by other authors (455°C for p_1 by Hamasumi [14] and 375°C for D,

Table 1
Experimental data for the ternary Al–Mg–Zn system in the literature

Reference	Experimental	Ternary	Type of data	Composition
[10]	Thermal analysis	τ^a	Liquidus	whole system
	Metallography		invar. equil.	
[26]	Thermal analysis		Liquidus, solidus	section Al–$MgZn_2$
	Metallography		(Al) solvus, invar. equil.	
[38]			(Al) solvus	
[39]	Thermal analysis		(Al) solvus	section Al–$MgZn_2$
	Metallography			
[11]	X-ray	τ^a	Crystal structure	$Mg_3Zn_3Al_2$ (τ)
[14]	Thermal analysis	τ^a	Liquidus	whole system
	Metallography		invar. equil.	
	X-ray		τ extension	
[15]	Thermal analysis	τ^a	Liquidus	Al–$Al_2Mg_3Zn_3$–$MgZn_2$–Zn
	Metallography			
[16]	Thermal analysis	τ^a	Liquidus	Al–Al_3Mg_4–$Al_2Mg_3Zn_3$–Al
	Metallography		invar. equil.	
[17]	Thermal analysis	τ^a	Liquidus	Mg–Al_3Mg_4–$Al_2Mg_3Zn_3$
	Metallography		invar. equil.	–$MgZn_2$–Mg
[48]	Electr. conductivity	τ^b	Phase boundaries	0–20Mg; 0–20Zn (mass%)
[49]	Metallography		containing (Al),	
	X-ray		β-Al–Mg and τ	
[18]	Metallography	τ^c	τ extension	τ-β, τ-γ, τ-Mg,
	X-ray		τ-$MgZn_2$, τ-(Al), Al–$MgZn_2$	
[40]	Thermal analysis		(Al) solvus	Al–$MgZn_2$
[21]	Metallography			
[27]	Thermal analysis		Liquidus	whole system
	Metallography		invar. equil.	
[28]	Thermal analysis		Liquidus	0–5Mg, 0–2Mn, 0–8Zn
	Metallography		invar. equil.	(mass%)
[41]	Metallography		(Al) solvus	
[42]				
[43]	Metallography		(Al) solvus	
[19]	Metallography	τ^c	τ extension	whole system
[29]	Thermal analysis		Liquidus, solidus	
	Metallography		(Al) solvus	
[30]	Thermal analysis		Liquidus	whole system
	Metallography		invar. equil.	
[47]	Metallography		(Mg) solvus	0–10Zn, 0–25Al (mass%)
[44]	Metallography		(Al) solvus, 460°C	0–17Mg, 0–17Zn (mass%)
[20]	Thermal analysis	τ^a	Liquidus,	Al–Zn–$MgZn_2$, Al–$MgZn_2$
	Metallography		Invar. equil.	Al_3Mg_4–$MgZn_2$–Mg
			τ extension	
[12]	X-ray	τ	Crystal structure	
[13]				
[35]	Metallography		Equil. Phases	0–8Mg, 0–8Zn (mass%)
[45]			(Al) solvus	0–20Mg, 0–20Zn (mass%)
[50]	Diffusion layer	Φ^d, τ^e	Equil. Phases	
[21]	Metallography		Φ and τ extension	
	X-ray			
[51]	Vapour pressure		Zn partial pressure	whole system
[46]			(Al) Solvus	0–40Mg, 0–40Zn (mass.%)
[31]	Thermal analysis		Liquidus	0–8Al, 0–8Mg (mass%)
	Metallography		Invar. equil.	

Table 1
(*Continued*)

Reference	Experimental	Ternary	Type of data	Composition
[52]	Vapour pressure		Zn partial pressure	whole system
[53]	EMF		Chemical potential of Mg in liquid	whole system
[36]	Thermal analysis Metallography		Liquidus, solidus	0–30Mg, 0–80Zn (mass.%)
[32]	Thermal analysis		Liquidus,	0–40Mg, 0–100Zn (mass%)
[37]	Metallography X-ray		(Al) solidus	
[22]	TEM	Φ	Φ extension, Unit cell	
[54]	Mixing calorimetry		Partial enthalpy	0–40Al, 0–20Mg 0–40Zn (at.%)

[a] Named ω in the original paper.
[b] Named α-(*Al–Mg–Zn*) in the original paper.
[c] Named T in the original paper.
[d] Name γ in the original paper.
[e] Named λ in the original paper.

Table 2
Crystal structures and phase descriptions

System	Phase	Prototype	Pearson symbol	Space group	Comments
Al	(Al)	Cu	cF4	$Fm\bar{3}m$	
Mg	(Mg)	Mg	hP2	$P6_3/mmc$	
Zn	(Zn)	Mg	hP2	$P6_3/mmc$	
Al–Mg	Al_3Mg_2	Al_3Mg_2	cF1832	$Fd\bar{3}$	β
	$Al_{30}Mg_{23}$	$Co_5Cr_2Mo_3$	hR53	$R\bar{3}$	ε
	$Al_{12}Mg_{17}$	αMn	cI58	$I\bar{4}3m$	γ
Mg–Zn	Mg_7Zn_3		oI142	*Immm*	$Mg_{51}Zn_{20}$
	MgZn				$Mg_{12}Zn_{13}$
	Mg_2Zn_3		mC110	B2/*m*	
	$MgZn_2$	$MgZn_2$	hP12	$P6_3/mmc$	Laves-C14
	Mg_2Zn_{11}	Mg_2Zn_{11}	cP39	$Pm\bar{3}$	
Al–Mg–Zn	Φ		orthorh.		
	τ	$Mg_{32}(Al,Zn)_{49}$	cI162	$Im\bar{3}$	

probably due to a misprint, in [15]). Moreover, the phase compositions related to the ternary peritectic formation of the Φ-phase given at 393°C by Petrov [9] disagree with a P-type reaction (the liquid phase composition is located within the triangle formed by the γ-Al–Mg, τ- and Φ-phases).

2.1.4. Solidus surface

Experimental determinations of the solidus surface [15–17,29,35–37] are all restricted to the Al-rich corner. Willey [7] gave a generalized solidus diagram of the Al corner of the system. The results of Stiller [36] and Kuznetsov et al. [37] agree very well with those of Willey [7].

2.1.5. Solvus

The solubility of Mg and Zn in (Al) was studied in several papers [26,29,38–46]. Most of these results are compared and presented in a partial solvus diagram by Willey [7].

The only determination of the Mg solvus was carried out in the range from 0 to 25 Al and 0 to 25 Zn (mass%) [47].

No experimental determination of the Zn solvus has been found in literature.

2.1.6. Isothermal sections

A complete isothermal section at 20°C, showing a large extension of the τ-phase, was first proposed by Köster and Dullenkopf [17]. A series of partial isothermal sections in the Al corner and adjoining the Al–Zn side were determined in the temperature range from 400°C to 200°C [41,42,48,49]. Of highest interest is the work of Clark [21] who constructed the isothermal section of the whole ternary system at 335°C and also proposed another two schematic isothermal sections at 394°C and 374°C. Willey [7] and Despande et al. [8] in their review work reproduced the isothermal section at 335°C from Clark [21].

2.2. Thermodynamic data

Thermodynamic data of the Al–Mg–Zn system are restricted to a few data on the liquid phase. Kozuka [51] and Lukashenko and Pogodaev [52] measured the vapour pressure of Zn in liquid by the carrier gas method. Pogodaev and Lukashenko [53] determined also Mg activities in liquid by EMF. Kim et al. [54] measured partial enthalpies of Al, Mg and Zn in Al–Mg–Zn melts by mixing calorimetry.

2.3. Thermodynamic assessment in literature

The Al–Mg–Zn system has been already thermodynamically evaluated by Chen [55]. However, in this assessment the ternary phases were simplified, the τ-phase was modelled as a line compound $Mg_{32}(Al,Zn)_{49}$ and the Φ-phase as a stoichiometric phase $Al_2Mg_5Zn_2$. The solubilities of Zn in the Al–Mg binary phases β, γ, ε and the Al solubilities in the Mg–Zn binary phases Mg_7Zn_3, MgZn, Mg_2Zn_3 and Mg_2Zn_{11} were neglected.

3. Experimental investigations

Literature research revealed lack of information about the ternary solubilities of the Al–Mg and Mg–Zn phases. Also the homogeneity ranges of τ and Φ were not very well known as well as the temperatures of some ternary invariant reactions.

Own experiments by X-ray diffraction (XRD), optical microscopy, Scanning Electron Microscopy (SEM), Transmission Electron Microscopy (TEM) and Electron Probe Micro Analysis (EPMA), Energy Dispersive X-ray spectroscopy (EDX) and Wave Dispersive X-ray Spectroscopy (WDX) were used to improve the knowledge on the homogeneity ranges as well as Differential Scanning Calorimetry (DSC) and Differential Thermal Analysis (DTA) to check the temperatures of some invariant reactions.

3.1. Experimental procedure

34 ternary alloys were prepared from high purity Mg (99.99%), Al (99.99%) and Zn (ca. 99.9%). Prealloying of the components previously weighed in the right proportions was carried out in a pure, nuclear quality graphite crucible placed inside a water-cooled copper crucible by induction melting under an helium atmosphere. Melting was repeated twice to ensure homogeneity of the ingot. A third final melting was carried out directly inside the water cooled copper crucible in order to obtain a cylindrical cast alloy of about 1 cm diameter and 5 cm height. During the melting process, the heating power was carefully controlled in order to avoid Zn and Mg loss by evaporation. Pieces from the cast alloys were sealed under argon in Pyrex ampoules, annealed at 335°C for at least 19 days and finally cooled to room temperature during about 10 min. The annealed samples were investigated by XRD using a Philips PK 1730/10 diffractometer with CoK_α radiation. The compositions of the annealed samples were determined by inductively coupled plasma/atomic emission spectroscopy (ICP). A comparison with the nominal compositions showed that the nominal compositions were within 1% of that determined by ICP. Phase compositions were determined by WDX. TEM observations were carried out with a Philips CM20 microscope at 120 and 200 kV on some specimens with compositions close to the Φ-phase [22].

The annealed samples were studied by DSC (Perkin-Elmer DSC-2C) under argon atmosphere. Each specimen (ca. 10 mg) was powdered and then hermetically encapsulated inside small Al crucibles (3 mm

Table 3
DSC or DTA* temperatures (in K)

Composition in at.%			Onset temperatures, endothermic effects observed on heating			
Al	Mg	Zn	1st effect	other effects		
50	40	10	721(?)	724(s)	733(b)	736(sh)
43	44	13	719(s)	724(sh,b)		
43	40	17	737(s)	748(sh)	753(b)	
43	36	21	736*(s)	773*(s)		
43	32	25	746*(s)	783*(s)		
30	48	22	**665**(s,n)			
30	44	26	741(b)			
30	40	30	742(vw)			
30	32	38	**756**(s,n)			
28	54	18	**663**(s,n)			
28	52	20	**663**(s,n)			
25	55	20	**633**(s,n,vw)	659(s,n)		
20	60	20	632(s)	655(s)		
20	54	26	649(s)	653(sh)		
20	48	32	634(s)	738(b)		
20	44	36	630(s)	740(b)		
20	40	40	748(b)			
20	36	44	**799***(s,n)			
20	32	48	**752**(s,n)			
18	40	42	748(s)			
18	36	46	**800***(s,n)			

The shape and intensity of the peaks is mentioned by abbreviations: (s) sharp; (n) narrow; (b) broad; (w) weak; (vw) very weak; (sh) shoulder; (?) questionable effect.
Bold faced values suggest invariant reactions.

high, 5 mm diameter)[1]. Covered Ta crucibles were also used for comparison. Specimens were rapidly heated (80 K/min) to 335°C and then slowly heated (1.25 K/min) to 500°C. Temperature calibration was carried out using the onset melting temperature of lead and zinc, according to the IUPAC, ICTA recommendations. For the invariant reactions occurring above 500°C, DTA (SETARAM, microthermal analyzer) was used at a heating rate of about 20 K/min. Specimens (ca. 10–20 mg) were put in open alumina crucibles and heated in flowing argon. As a heating rate of 20 K/min is too high to allow equilibrium melting, the only temperatures listed are those for the first and sharp endothermic event. Some of the temperatures of the invariant reactions thus measured were used as input data for the calculation.

[1]The formation of an adherent and non-porous alumina layer on the surface of the Al crucible avoids any contact between the Al–Mg–Zn alloy and Al. No reaction occurs between the specimen and the crucible when the upper limit temperature of the experiment remains lower than 500°C.

3.2. Experimental results

Table 3 shows the DSC and DTA results:

(i) The invariant pseudo-binary peritectic reaction $L+MgZn_2 \rightleftharpoons \tau$ is experimentally determined at about 800 K by DTA for two alloys, $Al_{20}Mg_{36}Zn_{44}$ (799 K) and $Al_{18}Mg_{36}Zn_{46}$ (800 K);
(ii) The invariant pseudo-binary eutectic reaction $L \rightleftharpoons (Al)+\tau$ is experimentally determined by DSC at 756 K for the alloy $Al_{30}Mg_{32}Zn_{38}$;
(iii) The peritectic formation of the Φ-phase by the reaction $L+\gamma+\tau \rightleftharpoons \Phi$ is determined at about 663 K by DSC with 4 alloys, $Al_{30}Mg_{48}Zn_{22}$ (665 K), $Al_{28}Mg_{52}Zn_{20}$ (663 K), $Al_{28}Mg_{54}Zn_{18}$ (663 K), $Al_{25}Mg_{55}Zn_{20}$ (659 K), with a maximal deviation of 6 K;
(iv) The existence of a transition reaction $L+\gamma \rightleftharpoons (Mg)+\Phi$ at 633 K is weakly (as expected) detected by DSC with the alloy $Al_{25}Mg_{55}Zn_{20}$.

Table 4
Phase compositions determined by WDX/EDX in Al–Mg–Zn alloys

Weighted elements(at.%)			Annealing treatment		Phase	Phase composition (at.%)		
Al	Mg	Zn	T(°C)	time		Al	Mg	Zn
30	40	30	335	19d	τ	30.2±0.3	41.0±0.2	28.8±0.3
43	40	17	335	19d	τ	42.8±0.3	40.3±0.3	16.9±0.1
50	40	10	335	19d	τ	49.0±0.3	40.2±0.2	10.8±0.8
					β-Al–Mg	56.6±0.2	38.8±0.1	4.6±0.2
20	40	40	335	19d	τ	20.5±0.1	39.9±0.5	39.6±0.5
18	40	42	335	19d	τ	18.5±0.1	39.8±0.2	41.7±0.2
30	48	22	335	19d	τ	31.1±0.1	43.0±0.2	25.9±0.2
					Φ	28.7±0.1	53.7±0.1	17.6±0.1
					γ-Al–Mg	33.9±0.3	57.7±0.2	8.4±0.3
30	44	26	335	19d	τ	30.2±0.4	43.1±0.2	26.7±0.2
					Φ	27.7±0.2	53.5±0.1	18.8±0.2
30	36	34	335	19d	τ	30.2±0.1	35.6±0.1	34.2±0.2
30	32	38	335	19d	τ	24.1±0.3	34.4±0.3	41.5±0.5
					(Al)			
20	44	36	335	19d	τ	20.4±0.1	41.7±0.2	37.9±0.2
					Φ	18.8±0.1	53.0±0.1	28.2±0.1
20	36	44	335	19d	τ	20.4±0.1	35.9±0.2	43.7±0.2
20	32	48	335	19d	τ	18.8±0.8	32.9±0.1	48.3±0.2
					Laves-C14	7.9±0.0	33.0±0.3	59.1±0.3
					(Al)	89.0±6.0	5.1±2.6	7.9±3.4
18	36	46	335	19d	τ	18.0±0.6	35.9±0.3	46.1±0.7
					Laves-C14	6.7±0.3	33.0±0.3	60.3±0.3
20	54	26	335	19d	Φ	20.1±0.1	54.1±0.2	25.8±0.2
					(Mg)	3.6±0.2	93.8±0.3	2.6±0.1
43	44	13	335	19d	τ	41.7±0.2	42.6±0.1	15.7±0.2
					γ-Al–Mg	44.0±0.1	45.6±0.1	10.4±0.1
43	36	21	335	19d	τ	40.6±0.2	37.6±0.1	15.8±0.1
					(Al)	93.2±0.3	5.7±0.3	1.1±0.0
43	32	25	335	19d	τ	35.1±0.1	36.6±0.2	28.2±0.2
					(Al)	93.5±0.5	4.7±0.4	1.8±0.2
20	60	20	335	19d	Φ	22.6±0.2	54.6±0.2	22.8±0.1
					(Mg)	3.9±0.2	93.8±0.3	2.3±0.1
28	52	20	335	19d	Φ	27.4±0.1	53.3±0.3	19.3±0.3
					τ	39.6±0.3	43.4±0.8	27.0±0.5
25	55	20	335	19d	Φ	25.2±0.2	55.0±0.2	19.9±0.3
28	54	18	335	19d	Φ	27.9±0.1	54.2±0.1	19.9±0.1
					γ-Al–Mg	31.8±0.6	57.2±0.4	11.0±0.8
58	40	2	400	10d	β-Al–Mg	56.9±0.2	41.2±0.2	1.9±0.1
					ϵ-Al–Mg	52.6±0.4	44.95±0.4	2.2±0.5
35	53	12	400	10d	τ	34.0±0.4	47.8±0.3	18.2±0.2
					γ-Al–Mg	34.6±0.2	58.0±0.3	7.4±0.2
2	15	83	300	14d	Mg_2Zn_{11}	2.1±0.1	16.4±0.2	81.5±0.1
					(Zn)	1.7±0.2	0.13±0.0	97.8±0.8
2	33	65	300	14d	Laves-C14	2.1±0.1	35.0±0.9	63.0±0.9
2	40	58	300	14d	Mg_2Zn_3	1.4±0.1	37.8±0.1	60.8±0.1
					MgZn	2.8±0.1	49.7±0.4	47.5±0.4
2	48	50	300	14d	MgZn	2.0±0.1	50.1±0.3	47.9±0.3
5	45	58	335	10d	Mg_2Zn_3	5.9±0.2	42.3±0.3	51.8±0.4
					MgZn	5.3±0.1	48.7±0.3	46.0±0.3
30	50	20	335	10d	τ	32.5±1	45.3±0.4	22.7±0.2
					γ-Al–Mg	35.5±0.2	56.9±0.2	7.5±0.2
					Φ	29.7±0.4	54.4±0.4	15.8±0.2

Table 4
(*Continued*)

Weighted elements(at.%)			Annealing treatment		Phase	Phase composition (at.%)		
Al	Mg	Zn	T(°C)	time		Al	Mg	Zn
10	55	35	335	10d	τ	15.2±0.8	43.1±0.5	41.8±0.9
					MgZn	9.6±0.4	49.2±0.5	41.3±0.3
					(Mg)	(4.0)	(92)	(4.0)
58	35	7	335	10d	(Al)	(90.0)	(9.1)	(0.9)
					β-Al–Mg	56.5±0.4	37.8±0.3	5.7±0.2
					τ	49.4±0.6	38.2±0.2	12.5±0.5
18	15	67	335	10d	Laves-C14	2.3±0.1	33.0±0.3	64.7±0.2
					Mg_2Zn_{11}	3.3±0.1	16.1±0.2	80.6±0.1
					(Al)	42.4±0.5	0.7±0.6	57.0±0.3
10	40	50	335	10d	Mg_2Zn_3	6.9±0.1	40.4±0.1	52.7±0.1
					τ	13.0±0.1	40.6±0.1	46.6±0.1
10	40	50	335	10d	Φ	29.3±0.1	53.7±0.2	17.0±0.2
					γ-Al–Mg	34.7±0.1	57.1±0.2	8.2±0.1

The other thermal events detected by DSC correspond to heat effects evolved on crossing phase boundaries.

The phase compositions determined by EPMA are given in Table 4. These data are also shown in Fig. 5.

4. Thermodynamic assessment

Due to new experimental measurements [56,57], revision of the already evaluated binary subsystems Al–Mg [2] and Mg–Zn [3] was desirable.

4.1. The Al–Mg system

Experimental work on the central part of the Al–Mg phase diagram between the β-(Al_3Mg_{2-}) and γ-($Al_{12}Mg_{17-}$) phases [56] could not confirm exactly the diagram reproduced by Hansen and Anderko [58] nor those of Massalski [59], Chartrand et al. [60] or Schürmann [61], which was accepted by Petrov [9]. The temperature range of stability of the ε-phase was found at lower temperatures than reported by Schürmann [61].

It is suggested that the phase denoted as ζ, $Al_{49}Mg_{32}$, by Schürmann should be related either to the sequence of metastable quasiperiodic phases which occur in this composition range [62] or to the commensurately modulated states related to the gamma phase, recently described by Donnadieu et al. [63].

In the present work the γ-phase model of Saunders [2] was changed to satisfy the suggestions made by Ansara et al. [64]. As described in Table 5, the sites occupied by Mg in the ideal formula $Al_{12}Mg_{17}$ have coordination numbers of 16 or 13. On substitution the

Table 5
Crystallography of the γ-$Al_{12}Mg_{17}$ phase [64]

Prototype	αMn			
Space group	I $\bar{4}$3 m			
Pearson symbol	cI58			
Wyckoff notation	2(a)	8(c)	24(g)	24(g)
Point symmetry	$\bar{4}3m$	3m	m	m
Coordination No.	16	16	13	12
Ideal site occupation	Mg	Mg	Mg	Al
Model site occupation	Mg	Mg	(**Mg**, Al)	(**Al**, Mg)

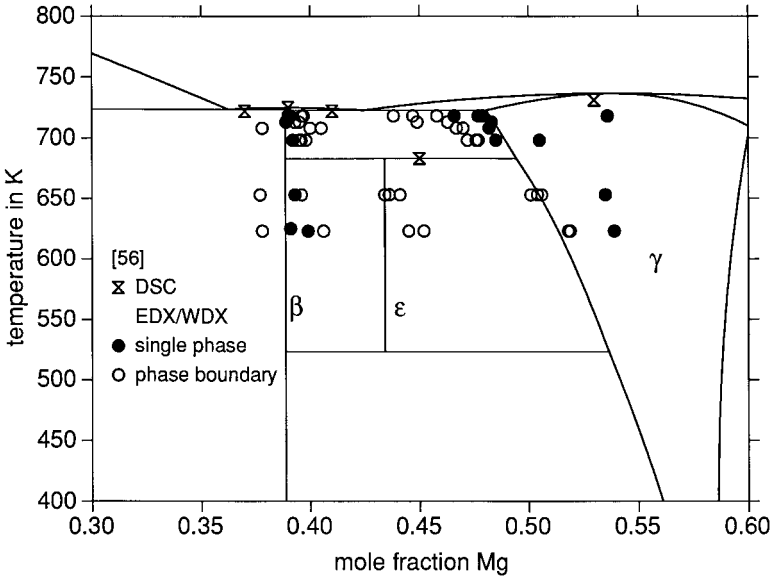

Fig. 1. Central part of the Al–Mg phase diagram.

13 fold coordinated Mg atoms are more likely replaced by Al than the 16 fold coordinated ones. Therefore in the compound energy formalism this phase was modelled as Mg_{10}(**Mg**, Al)$_{24}$(**Al**, Mg)$_{24}$, where boldface denotes the major constituents.

The intermediate phases of this system were re-optimized by trial and error keeping the descriptions of Saunders [2] for the liquid phase and for the Al(fcc) and Mg(hcp) solid solutions. The β- and ε-phases were treated as stoichiometric phases with Al:Mg ratios 140:89 and 30:23 respectively. These ratios take into account the total number of lattice sites and the mean compositions of the homogeneity ranges, although, at least in β, the site occupation is less well defined. The central part of the phase diagram, calculated with the resulting parameters, is shown in Fig. 1.

4.2. The Mg–Zn system

In the Mg–Zn system Gödecke and Sommer [57] measured C_p^{liquid} at 28.1 at.% Zn between 650 and 750 K (Fig. 2). The results confirm the large positive deviation from Kopp–Neumann's rule derived by Agarwal et al. [3] from the temperature dependence of the enthalpy of mixing of the liquid, but the numerical value of this deviation is refined to about 70% of that assessed by Agarwal et al. [3].

Kowalski and Spencer [65] in the Cu–Zn system assumed different lattice stabilities for pure Zn in its stable state (hcp with c/a=1.856) and as hcp phase with axial ratio c/a=1.556 (ε-Cu–Zn phase), which lies close to the ideal axial ratio c/a=1.633. To get compatibility, in Mg–Zn the Mg(hcp) solid solution had to be reformulated to show the same lattice stability for the end member pure Zn as Kowalski and Spencer [65] used for the ε-Cu–Zn phase.

Furthermore the $MgZn_2$ (Laves-C14) phase should be modelled similarly as $MgCu_2$ with anti-structure atom formation on both sublattices (**Mg**, Zn)$_1$(**Zn**, Mg)$_2$, although the only information for that is the statement: "The homogeneity range of $MgZn_2$ is 66 to 67.1 at.% Zn" [59]. For the Gibbs energy parameters $G^{MgZn_2}_{Mg:Mg}$ and $G^{MgZn_2}_{Zn:Zn}$ of the end members "pure elements in the Laves phase structure" a value of +15000 J/mol (5000 J/(mol of atoms)), as used for other Laves phases [66,67], was chosen.

The Mg–Zn system was re-optimized using the existing experimental-data file of [3] updated by the C_p^{liquid} data [57]. The Laves phase parameters ${}^0L^{MgZn_2}_{Mg:Zn,\,Mg}$ and ${}^0L^{MgZn_2}_{Mg,\,Zn:Zn}$ were estimated by trial and error to reproduce the homogeneity range reported by Massalski [59].

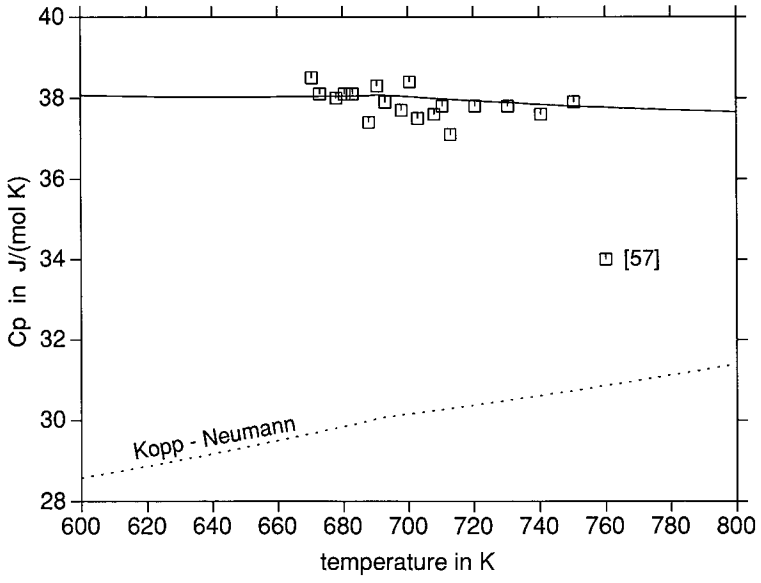

Fig. 2. Cp of a liquid Mg–Zn alloy at 28.1 at.% Zn.

4.3. The Al–Mg–Zn system

The optimization of the Al–Mg–Zn ternary system incorporates, in addition to the available published data, the experimental data described in Section 3.

4.3.1. Thermodynamic modelling

The thermodynamic descriptions of the pure elements in the present work are accepted from the SGTE (Scientific Group Thermodata Europe) databank [68].

4.3.1.1. Liquid phase and (Al), (Mg), (Zn) solid solutions:. The liquid phase, the (Al), (Mg) and (Zn) solid solutions were described as substitutional solutions by the Redlich–Kister–Muggianu formalism.

4.3.1.2. τ-phase:. The ternary τ-phase has a large homogeneity region. Its ideal formula is $Mg_{32}(Zn, Al)_{49}$. Details of its crystal structure are given in Table 6, including the site occupations determined in a single phase alloy [12].

The homogeneity range of τ extends to areas more rich and more poor in Mg than given by the ideal formula $Mg_{32}(Al, Zn)_{49}$. Therefore Mg occupation in the Al–Zn sublattices as well as Al and/or Zn occupation in Mg sublattices must be considered. As the Al–Zn sublattices all have the same coordination No. and their Al–Zn occupation is only moderately different, they were treated as a single sublattice with Al and Zn as major and Mg as minor constituents, except the position 2(a), which contains only Al according to [12].

For the Mg sublattices the 14 fold coordinated position 12(e) is more likely substituted than the 15 and 16 fold coordinated positions. To simplify the model only substitution by Al is considered. As the mutual solubilities of Mg and Al in the Al–Mg binary system are larger than those of Mg and Zn in the Mg–Zn binary system, this assumption is not unrealistic. The resulting model thus is:

$(\mathbf{Mg})_{26}(\mathbf{Mg}, Al)_6(\mathbf{Al}, \mathbf{Zn}, Mg)_{48}(\mathbf{Al})_1$

It is worth to note, that the τ-phase is isotypic with the T-phase in the ternary Al–Cu–Mg system and the τ- and T-phases form continuous solid solutions in the quaternary Al–Cu–Mg–Zn system [13,33,44]. To describe the quaternary extension, it is thus necessary to use the same model for both phases, even in the ternaries. Therefore the T-phase in the ternary Al–Cu–Mg was modelled as $(\mathbf{Mg})_{26}(\mathbf{Mg}, Al)_6(\mathbf{Al}, Cu, Mg)_{48}(\mathbf{Al})_1$ [4]. The model $(\mathbf{Mg})_{26}(\mathbf{Mg}, Al)_6(\mathbf{Al}, \mathbf{Zn}, Cu, Mg)_{48}(\mathbf{Al})_1$ enables to describe the τ- and T-phases as well as the quaternary extension.

Table 6
Crystallography of the τ-Phase in the Al–Mg–Zn System [12]

Position	16(f)	24(g)	12(e)	12(e)	24(g)	24(g)	48(h)	2(a)
Occupation[12]	Mg	Mg	Mg	Mg	Zn(83)+Al(17)	Al(56)+Zn(44)	Al(52)+Zn(48)	Al
Coord. No.	16	16	15	14	12	12	12	12
Modelling	**Mg**	**Mg**	**Mg**	(**Mg**, Al)	(**Al**, **Zn**, Mg)	(**Al**, **Zn**, Mg)	(**Al**, **Zn**, Mg)	**Al**

$Mg_{32}(Al,Zn)_{49}$, Pearson symbol: cI162, Space group: $Im\bar{3}$.

4.3.1.3. Φ-phase:. The unit cell of the ternary Φ-phase was recently determined by electron diffraction in a transmission electron microscope [22]. It is orthorhombic, space group $Pbc2_1$, or Pbcm with large lattice parameters (a=897.9, b=1698.8, c=1934 pm). As no further details on its structure are known it was modelled by the sublattice formula $Mg_6(Al,Zn)_5$. This formula reproduces the experimental facts, a nearly fixed Mg content of about 54.5 at.% and an extended homogeneity range along Al to Zn exchange.

4.3.1.4. Al–Mg and Mg–Zn binary intermetallic phases:. The experimental results (EPMA) show that the Al–Mg as well as the Mg–Zn binary phases exhibit ternary solubilities to several at.%. As Al–Zn substitution seems more likely than Al–Mg or Mg–Zn substitution, these binary phases with ternary solubilities were modelled as follows, starting from the already used binary descriptions:

β-AlMg: Mg_{89}(**Al**, Zn)$_{140}$ ε-AlMg: Mg_{23}(**Al**, Zn)$_{30}$ γ-AlMg: Mg_{10}(**Mg**, Al, Zn)$_{24}$(**Al**, Mg, Zn)$_{24}$ Mg_2Zn_{11}: Mg_2(**Zn**, Al)$_{11}$ $MgZn_2$: (**Mg**, Al, Zn)(**Zn**, Al, Mg)$_2$ Mg_2Zn_3: Mg_2(**Zn**, Al)$_3$ MgZn: Mg_{12}(**Zn**, Al)$_{13}$.

The major constituents are denoted in boldface. Mg_7Zn_3 was treated as stoichiometric phase. A similar treatment as for the other phases would be logical, but would not change anything significantly, as this phase is stable between 614 and 598 K only. Also there are no experimental data on its Al-solubility.

4.3.2. Selection of the adjustable parameters

4.3.2.1. Liquid phase:. The partial enthalpy measurements of Al, Mg and Zn in Al–Mg–Zn melts [54] enable to adjust the temperature independent part of a ternary term $x_{Al}x_{Mg}x_{Zn}{}^0L^{liquid}_{Al,Mg,Zn}$. A linearly temperature dependent part can be adjusted to the measured partial Gibbs energies of Mg and Zn in Al–Mg–Zn melts [51–53].

4.3.2.2. (Al), (Mg) and (Zn) solid solutions:. For the solid solutions no ternary parameters were used, as the simultaneous solubility of two elements is small everywhere in these phases. Thus their Gibbs energies are fully determined by the binary descriptions. As these phases do not exist in all three binary systems, however, there are no binary descriptions for fcc-A1 in the Mg–Zn system, hcp-A3 in the Al–Zn system and hcp-Zn in the Al–Mg system. They had to be estimated. These parameters are always multiplied with the product of two small site fractions, therefore they have only very small influence on the calculated Gibbs energies. The corresponding parameters of stable solid solutions of the same system were taken as estimates for the missing ones: ${}^vL^{fcc-A1}_{Mg,Zn} = {}^vL^{hcp-A3}_{Mg,Zn} = {}^vL^{hcp-Zn}_{Mg,Zn}$ and ${}^vL^{hcp-Zn}_{Al,Mg} = {}^vL^{hcp-A3}_{Al,Mg}$.

4.3.2.3. τ-phase:. The model $(Mg)_{26}$(**Mg**,Al)$_6$-(**Al**,**Zn**,Mg)$_{48}$(Al)$_1$ for the τ-phase requires Gibbs energies of formation parameters for 6 metastable end members, i.e. the six parameters:

$$
\begin{aligned}
{}^0G^{\tau}_{Mg:Mg:Al:Al} &= 49\,{}^0G^{fcc}_{Al} + 32\,{}^0G^{hcp}_{Mg} \\
{}^0G^{\tau}_{Mg:Mg:Zn:Al} &= {}^0G^{fcc}_{Al} + 32\,{}^0G^{hcp}_{Mg} - 48\,{}^0G^{hcp}_{Zn} \\
{}^0G^{\tau}_{Mg:Mg:Mg:Al} &= {}^0G^{fcc}_{Al} + 80\,{}^0G^{hcp}_{Mg} \\
{}^0G^{\tau}_{Mg:Al:Al:Al} &= 55\,{}^0G^{fcc}_{Al} + 26\,{}^0G^{hcp}_{Mg} \\
{}^0G^{\tau}_{Mg:Al:Zn:Al} &= 7\,{}^0G^{fcc}_{Al} + 26\,{}^0G^{hcp}_{Mg} - 48\,{}^0G^{hcp}_{Zn} \\
{}^0G^{\tau}_{Mg:Al:Mg:Al} &= 7\,{}^0G^{fcc}_{Al} + 74\,{}^0G^{hcp}_{Mg}
\end{aligned}
$$

The first five parameters can be independently adjusted. Between the first two there is a large range of stability of the phase, they have to be adjusted precisely. The third one describes mainly

the Mg rich limit of τ. The fourth and fifth parameters describe the Mg poor limit of the homogeneity range independently at the Al and Zn rich ends respectively. The sixth one is not significant, as it describes a state where the second as well as the third sublattice is occupied by antistructure atoms. Therefore it must have a large positive value.

Besides these Gibbs energy parameters of the end members of the compound energy formalism, some interaction parameters were introduced. ${}^{0}L^{\tau}_{\mathrm{Mg:Mg:Al,\,Mg:Al}}$ and ${}^{0}L^{\tau}_{\mathrm{Mg:Mg:Mg,\,Zn:Al}}$ enable to describe the Mg-rich boundary differently in the Al rich and Zn rich part. The corresponding two parameters with Al on the second sublattice were set equal to those with Mg on the second sublattice. Although they are not significant, this solution is more natural than setting them zero.

The parameters ${}^{0}L^{\tau}_{\mathrm{Mg:Mg:Al,\,Zn:Al}}$ and ${}^{0}L^{\tau}_{\mathrm{Mg:Al:Al,\,Zn:Al}}$ describe the shape of the G vs. x curve of τ along the largest extension of the homogeneity range. They were independently adjusted, which enables the independent modelling of the curvature of the Mg poor and Mg rich boundary of the homogeneity range.

The EPMA data provide values of the boundary of the homogeneity range around τ at 608 K and this allows to adjust relations between these parameters mainly connected with the shape of the $G^{\tau}(x_i)$ curves.

The value of the Gibbs energy of τ relative to the standard states is also reflected in the solubility limits of the phases in equilibrium with τ. Especially the calculated values of the solvus of the (Al) solid solution react sensitively on the magnitude of G^{τ}. The Gibbs energy of the (Al) solid solution is well defined by the Muggianu extrapolation of its binary descriptions and deviation from this extrapolation can be modelled by ternary parameters only in very limited amounts. As there are no strong arguments against the Redlich–Kister–Muggianu description for the (Al) solid solution, the experimental values of the (Al) solvus can be reproduced only by correct modelling of the magnitude of G^{τ}.

4.3.2.4. Φ-phase:. For the ternary Φ-phase three parameters were used: ${}^{0}G^{\Phi}_{\mathrm{Mg:Al}}$, ${}^{0}G^{\Phi}_{\mathrm{Mg:Zn}}$ and ${}^{0}G^{\Phi}_{\mathrm{Mg:Al,\,Zn}}$, all as linear functions of temperature.

4.3.2.5. Laves-C14 phase:. The Laves-C14 phase forms continuous solid solutions in the quaternary system Al–Cu–Mg–Zn from $MgZn_2$ to about AlCuMg [33,44]. The model (**Mg**, Al, Cu, Zn)(**Cu**, **Zn**, Al, $Mg)_2$ enables to describe mixing in the quaternary system. To allow combination of the ternary descriptions for the quaternary system, the parameters ${}^{0}G^{\mathrm{Laves-C14}}_{\mathrm{Mg:Al}}$, ${}^{0}G^{\mathrm{Laves-C14}}_{\mathrm{Al:Mg}}$, ${}^{0}L^{\mathrm{Laves-C14}}_{\mathrm{Mg:Al:*}}$, ${}^{0}L^{\mathrm{Laves-C14}}_{\mathrm{*:Mg,\,Al}}$, were taken from [4]. The three parameters ${}^{0}L^{\mathrm{Laves-C14}}_{\mathrm{*:Al,Zn}}$, where "*" stands for Mg, Al or Zn, were set equal and treated in the optimization as a single parameter.

4.3.2.6. Al–Mg and Mg–Zn binary intermetallic phases:. To describe Zn solubilities in the β-Al–Mg and ε-Al–Mg phases, as well as **Al** solubilities in MgZn, Mg_2Zn_3 and Mg_2Zn_{11} only the Gibbs energy parameters of the fictive end members in the opposite binary systems were used.

For the γ-Al–Mg phase described by the model Mg_{10}(**Mg**, Al, Zn)$_{24}$(**Al**, Mg, Zn)$_{24}$ five such end members, ${}^{0}G^{\gamma-\mathrm{Al-Mg}}_{\mathrm{Mg:Zn:Al}}$, ${}^{0}G^{\gamma-\mathrm{Al-Mg}}_{\mathrm{Mg:Mg:Zn}}$, ${}^{0}G^{\gamma-\mathrm{Al-Mg}}_{\mathrm{Mg:Zn:Mg}}$, ${}^{0}G^{\gamma-\mathrm{Al-Mg}}_{\mathrm{Mg:Al:Zn}}$ and ${}^{0}G^{\gamma-\mathrm{Al-Mg}}_{\mathrm{Mg:Zn:Zn}}$ exist. Only the first two with major constituents on two sublattices, however, are significant. The third and fourth ones are related to the first and second ones respectively by the same antistructure occupation as the two binary Al–Mg parameters ${}^{0}G^{\gamma-\mathrm{Al-Mg}}_{\mathrm{Mg:Mg:Mg}}$ and ${}^{0}G^{\gamma-\mathrm{Al-Mg}}_{\mathrm{Mg:Al:Al}}$ are related to the parameter of "ideal" occupation, ${}^{0}G^{\gamma-\mathrm{Al-Mg}}_{\mathrm{Mg:Mg:Al}}$. Therefore they are expressed as:

$${}^{0}G^{\gamma-\mathrm{Al-Mg}}_{\mathrm{Mg:Zn:Mg}} = {}^{0}G^{\gamma-\mathrm{Al-Mg}}_{\mathrm{Mg:Zn:Al}} + {}^{0}G^{\gamma-\mathrm{Al-Mg}}_{\mathrm{Mg:Mg:Mg}} - {}^{0}G^{\gamma-\mathrm{Al-Mg}}_{\mathrm{Mg:Mg:Al}}$$

$${}^{0}G^{\gamma-\mathrm{Al-Mg}}_{\mathrm{Mg:Al:Zn}} = {}^{0}G^{\gamma-\mathrm{Al-Mg}}_{\mathrm{Mg:Mg:Zn}} + {}^{0}G^{\gamma-\mathrm{Al-Mg}}_{\mathrm{Mg:Al:Al}} - {}^{0}G^{\gamma-\mathrm{Al-Mg}}_{\mathrm{Mg:Mg:Al}}$$

For the fifth parameter a large positive value of 580000 J/mol (10000 J/(mol of atoms)) was arbitrarily chosen.

4.3.3. Thermodynamic optimization

The selected coefficients were adjusted to the experimental values by a combination of the "trial and error method" and the program TERGSS.

The description of all phases, but especially of the ternary τ-phase, is very complicated and the experimental information is still limited. Therefore it seems to be not satisfactory to use a single least squares calculation to adjust all parameters in one step. Moreover, many of the experimental data are specifically connected with single parameters and thus it seems natural to adjust these parameters separately using

mainly these data. That applies to all the ternary solubilities of binary phases.

4.3.3.1. Liquid phase:. In the first step ternary parameters of the Gibbs energy description of liquid were adjusted to the measurements of Kim et al. [54], Kozuka [51], Lukashenko and Pogodaev [52,53] using the least squares method by the program TERGSS. The enthalpy values of Kim are reported as integral enthalpies, but they also reported raw data enable the calculation of partial enthalpies. Partial enthalpies are defined as $\left(\frac{\partial H}{\partial N_j}\right)$ and approximated here by $\left(\frac{\Delta H}{\Delta N_j}\right)$, where ΔH is the measured heat effect and ΔN_j the amount of pure element j added to the liquid bath in the calorimeter. There is a composition between the compositions of the liquid bath before and after the measurement, where the quotient of differences is exactly equal to the differential quotient. This rule does not exactly locate the composition inside this interval, but that does not matter, as the intervals are small.

The integral enthalpies reported by Kim are calculated by summing up all measurements of a series, where successively small amounts of element j are added in the calorimeter to the same liquid bath. Using these integral enthalpy data in a least squares calculation would give wrong weight to the data points. The first measurement would appear in n data points, the second one in $n-1$ points and finally the last measurement would appear in only one data point and thus get much less weight in the calculation. Using the measurements as partial enthalpies in the least squares calculation, however, gives each data point the same weight. Furthermore a plot of the integral enthalpies calculated this way is very effectively smoothed, whereas a plot of partial enthalpies gives a much more realistic impression of the scatter of the measurements.

By the least squares method a single ternary term, $x_{Al}x_{Mg}x_{Zn}\,{}^{0}L^{liq}_{Al,Mg,Zn}$, was adjusted. The resulting calculated partial enthalpies of Zn are compared with the experimental values of Kim [54] in Fig. 3. The Mg partial enthalpies fit similarly well, those of Al fit a little worse. This figure also shows the good quality of the measurements, although there is no smoothing effect as in a plot of integral enthalpies. The ternary parameter significantly improves the fit

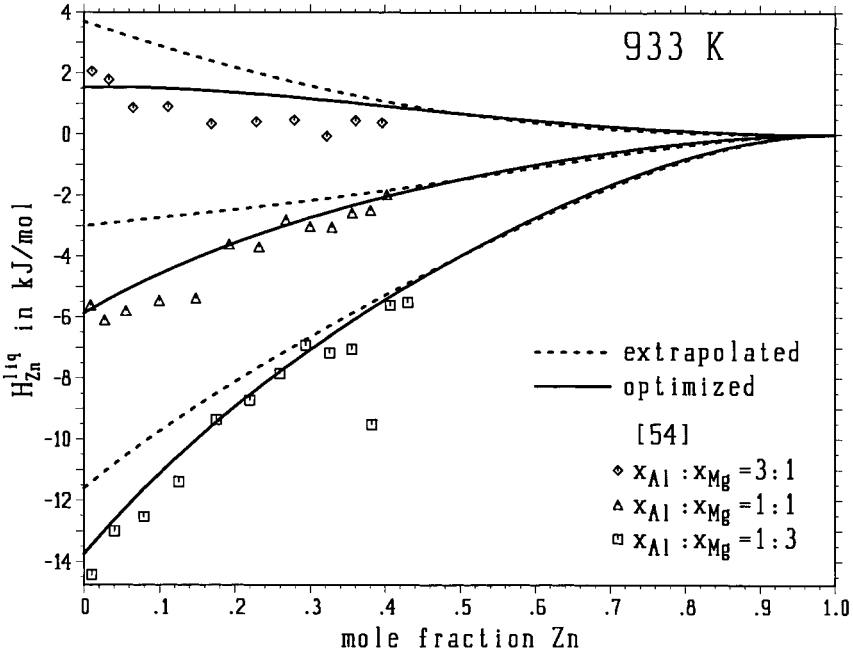

Fig. 3. Partial enthalpy of Zn in liquid Al–Mg–Zn alloys.

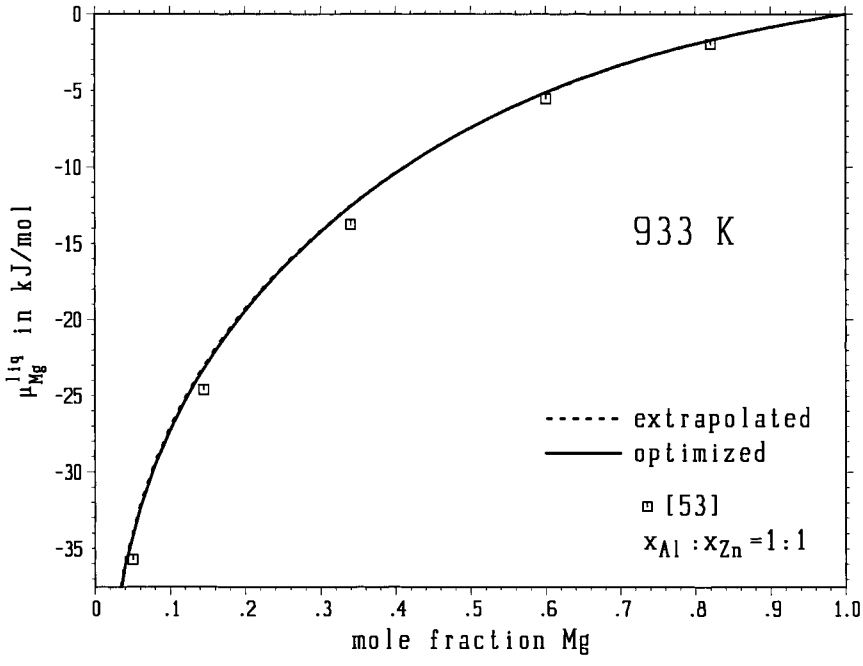

Fig. 4. Chemical potential of Mg in liquid Al–Mg–Zn alloys.

to the experimental data. A test with three ternary terms, $x_{Al}x_{Mg}x_{Zn}(x_{Al}\,{}^{1}L^{liq}_{Al,Mg,Zn} + x_{Mg}\,{}^{2}L^{liq}_{Al,Mg,Zn} + x_{Zn}\,{}^{3}L^{liq}_{Al,Mg,Zn})$, gave no significant further improvement.

Enthalpy measurements allow to adjust only the temperature independent part of the parameter ${}^{0}L^{liq}_{Al,Mg,Zn}$. A linearly temperature dependent part can be adjusted to measured chemical potential values [51–53]. In the optimized temperature dependent ternary parameter at the temperatures of measurement the entropy times T term nearly cancels the enthalpy term and thus the optimized Gibbs energy is nearly equal to the Muggianu extrapolation of the binary Gibbs energies as shown in Fig. 4. There from the μ^{liq}_{Mg} measurements of [53] the points falling onto a section with $x_{Al} : x_{Zn} = 1 : 1$ are compared with the calculated μ^{liq}_{Mg} values along this section.

4.3.3.2. τ-phase. The *G*-description of τ was adjusted by trial and error to fit the measurements of its solubility limits at 608 K and the temperature of its quasibinary peritectic formation, $L+MgZn_2 \rightleftharpoons \tau$.

First the Gibbs energy of the equilibrium mixture of the phases without τ was calculated at 608 K along a section Mg:(Al+Zn)=32:49, using the stable solid pure elements at the same temperature as reference states. Then the parameters ${}^{0}G^{\tau}_{Mg:Mg:Al:Al} - 49\,{}^{0}G^{fcc}_{Al} - 32\,{}^{0}G^{hcp}_{Mg}$ and ${}^{0}G^{\tau}_{Mg:Mg:Zn:Al} - {}^{0}G^{fcc}_{Al} - 32\,{}^{0}G^{hcp}_{Mg} - 48\,{}^{0}G^{hcp}_{Zn}$ were set to values slightly more positive than the corresponding *G*-values calculated with suspended τ-phase and adjusted to fit to the maximum Al and Zn solubilities of τ without using an interaction parameter for τ. The same was done for 273 K. The parameter values at the two different temperatures now were expressed by single linearly temperature dependent parameters.

Then the temperature of the quasibinary peritectic formation was calculated using these two parameters and the previously adjusted description of G^{liq} together with the binary Mg–Zn description of the C14 Laves phase. This temperature had to be adjusted to the experimental value of slightly above 800 K and simultaneously the solubility of Al in the C14 Laves phase was adjusted to about 5 at.% by interaction parameters ${}^{0}L^{\tau}_{Mg:Mg:Al,Zn:Al}$ and ${}^{0}L^{Laves-C14}_{Mg:Al,Zn}$. The pre-

Table 7
Parameter set for the Al–Mg–Zn system. Parameters are given as $a+bT+cTln\,(T)+dT^2+e/T+fT^3$ in J mol^{-1}. (per moles of formula units)

Parameter	*a*	*b*	*c*	*d*	Reference
Liquid, Redlich–Kister–Muggianu					
${}^0L^{liq}_{Al,Mg}$	−12000.00	8.56600			[2]
${}^1L^{liq}_{Al,Mg}$	1894.00	−3.00000			[2]
${}^2L^{liq}_{Al,Mg}$	2000.00				[2]
${}^0L^{liq}_{Al,Zn}$	10465.55	−3.39259			[69]
${}^0L^{liq}_{Mg,Zn}$	−77729.24	680.52266	−95	0.04	this work
${}^1L^{liq}_{Mg,Zn}$	3674.72	0.57139			this work
${}^2L^{liq}_{Mg,Zn}$	−1588.15				this work
${}^0L^{liq}_{Al,Mg,Zn}$	−11475.00	11.00000			this work
${}^1L^{liq}_{Al,Mg,Zn}$	−11475.00	11.00000			this work
${}^2L^{liq}_{Al,Mg,Zn}$	−11475.00	11.00000			this work
Al (fcc) solid solution, Redlich–Kister–Muggianu					
${}^0L^{fcc}_{Al,Mg}$	4971.00	−3.50000			[2]
${}^1L^{fcc}_{Al,Mg}$	900.00	0.42300			[2]
${}^2L^{fcc}_{Al,Mg}$	950.00				[2]
${}^0L^{fcc}_{Al,Zn}$	7297.48	0.47512			[69]
${}^1L^{fcc}_{Al,Zn}$	6612.88	−4.5911			[69]
${}^2L^{fcc}_{Al,Zn}$	−3097.19	3.30635			[69]
${}^0L^{fcc}_{Mg,Zn}$	−3056.82	5.63801			this work
${}^1L^{fcc}_{Mg,Zn}$	−3127.26	5.65563			this work
Zn (hcp-Zn) solid solution, Redlich–Kister–Muggianu					
${}^0G^{hcp-Zn}_{Al} - {}^0G^{fcc}_{Al}$	5581.00	−1.80000			[68]
${}^0G^{hcp-Zn}_{Mg} - {}^0G^{hcp}_{Mg}$	100.00				this work
${}^0L^{hcp-Zn}_{Al,Mg}$	1950.00	−2.00000			[2]
${}^1L^{hcp-Zn}_{Al,Mg}$	1480.00	−2.08000			[2]
${}^2L^{hcp-Zn}_{Al,Mg}$	3500.00				[2]
${}^0L^{hcp-Zn}_{Al,Zn}$	18820.95	−8.95255			[69]
${}^3L^{hcp-Zn}_{Al,Zn}$	−702.79				[69]
${}^0L^{hcp-Zn}_{Mg,Zn}$	−3056.82	5.63801			this work
${}^1L^{hcp-Zn}_{Mg,Zn}$	−3127.26	5.65563			this work
Mg (hcp-A3) solid solution; Redlich–Kister–Muggianu,					
${}^0G^{hcp-A3}_{Al} - {}^0G^{fcc}_{Al}$	5581.00	−1.80000			[68]
${}^0G^{hcp-A3}_{Zn} - {}^0G^{hcp}_{Zn}$	2969.82	−1.56968			[65]
${}^0L^{hcp-A3}_{Al,Mg}$	1950.00	−2.00000			[2]
${}^1L^{hcp-A3}_{Al,Mg}$	1480.00	−2.08000			[2]
${}^2L^{hcp-A3}_{Al,Mg}$	3500.00				[2]
${}^0L^{hcp-A3}_{Al,Zn}$	18820.95	−8.95255			[69]
${}^3L^{hcp-A3}_{Al,Zn}$	-702.79				[69]
${}^0L^{hcp-A3}_{Mg,Zn}$	−3056.82	5.63801			this work
${}^1L^{hcp-A3}_{Mg,Zn}$	−3127.26	5.65563			this work

Table 7
(*Continued*)

Parameter	*a*	*b*	*c*	*d*	Reference
β-Al_3Mg_2; compound energy formalism, $(Mg)_{89}(Al,Zn)_{140}$					
${}^0G^{\beta}_{Mg:Al} - 89{}^0G_{Mg^{hcp}} - 140{}^0G^{fcc}_{Al}$	−246175.00	−675.55000			this work
${}^0G^{\beta}_{Mg:Zn} - 89{}^0G_{Mg^{hcp}} - 140{}^0G^{hcp}_{Zn}$	206100.00				this work
${}^0L^{\beta}_{Mg:Al,Zn}$	−1717500.00	343.50000			this work
ε-$Al_{30}Mg_{23}$; compound energy formalism, $(Mg)_{23}(Al, Zn)_{30}$					
${}^0G^{\varepsilon}_{Mg:Al} - 23{}^0G_{Mg^{hcp}} - 30{}^0G_{Al^{fcc}}$	−52565.40	−173.17750			this work
${}^0G^{\epsilon}_{Mg:Zn} - 23{}^0G^{hcp}_{Mg} - 30{}^0G^{hcp}_{Zn}$	−318000.00	−63.60000			this work
γ-$Al_{12}Mg_{17}$; compound energy formalism, $(Mg)_{10}(Mg,Al,Zn)_{24}(Al,Mg,Zn)_{24}$					
${}^0G^{\gamma}_{Mg:Al:Al} - 10{}^0G^{hcp}_{Mg} - 48{}^0G^{fcc}_{Al}$	195750.00	−203.00000			this work
${}^0G^{\gamma}_{Mg:Mg:Al} - 34{}^0G^{hcp}_{Mg} - 24{}^0G^{fcc}_{Al}$	−105560.00	−101.50000			this work
${}^0G^{\gamma}_{Mg:Al:Mg} - 34{}^0G^{hcp}_{Mg} - 24{}^0G^{fcc}_{Al}$	568249.20	−276.13800			this work
${}^0G^{\gamma}_{Mg:Mg:Mg} - 58{}^0G^{hcp}_{Mg}$	266939.20	−174.63800			this work
${}^0G^{\gamma}_{Mg:Zn:Al} - 10{}^0G^{hcp}_{Mg} - 24{}^0G^{fcc}_{Al} - 24{}^0G^{hcp}_{Zn}$	−174000.00	116.00000			this work
${}^0G^{\gamma}_{Mg:Mg:Zn} - 34{}^0G^{hcp}_{Mg} - 24{}^0G^{hcp}_{Zn}$	−290000.00	116.00000			this work
${}^0G^{\gamma}_{Mg:Zn:Mg} - 34{}^0G^{hcp}_{Mg} - 24{}^0G^{hcp}_{Zn}$	198599.20	42.86200			this work
${}^0G^{\gamma}_{Mg:Al:Zn} - 10{}^0G^{hcp}_{Mg} - 24{}^0G^{fcc}_{Al} - 24{}^0G^{hcp}_{Zn}$	11310.00	14.50000			this work
${}^0G^{\gamma}_{Mg:Zn:Zn} - 10{}^0G^{hcp}_{Mg} - 48{}^0G^{hcp}_{Zn}$	580000.00				this work
${}^0L^{\gamma}_{Mg:Al:Al,Mg} = {}^0L^{\gamma}_{Mg:Mg:Al,Mg} = {}^0L^{\gamma}_{Mg:Zn:Al,Mg}$	226200.00	−29.00000			this work
${}^0L^{\gamma}_{Mg:Mg:Zn:Al} = {}^0L^{\gamma}_{Mg:Mg,Zn:Mg} = {}^0L^{\gamma}_{Mg:Mg,Zn:Zn}$	−232000.00	116.00000			this work
Mg_2Zn_{11}; compound energy formalism, $Mg_2(Zn,Al)_{11}$					
${}^0G^{Mg_2}_{Mg:Zn}Zn_{11} - 2{}^0G^{hcp}_{Mg} - 11{}^0G^{hcp}_{Zn}$	−73818.32	18.45457			this work
${}^0G^{Mg_2}_{Mg:Al}Zn_{11} - 2{}^0G^{hcp}_{Mg} - 11{}^0G^{fcc}_{Al}$	130000.00	−26.00000			this work
Laves-C14, $MgZn_2$; compound energy formalism, (Al, Mg,Zn)(Al,Mg, Zn)$_2$					
${}^0G^{Laves-C14}_{*:*} - 3{}^0G^{SER}_{*}$	15000.00				this work
${}^0G^{Laves-C14}_{Mg:Al} - {}^0G^{hcp}_{Mg} - 2{}^0G^{fcc}_{Al}$	12671.10	16.80000			[4]
${}^0G^{Laves-C14}_{Zn:Al} - {}^0G^{hcp}_{Zn} - 2{}^0G^{fcc}_{Al}$	15000.00				this work
${}^0G^{Laves-C14}_{Al:Mg} - {}^0G^{fcc}_{Al} - 2{}^0G^{hcp}_{Mg}$	37328.90	−16.80000			[4]
${}^0G^{Laves-C14}_{Zn:Mg} - {}^0G^{hcp}_{Zn} - 2{}^0G^{hcp}_{Mg}$	65355.45	− 8.83886			this work
${}^0G^{Laves-C14}_{Al:Zn} - {}^0G^{fcc}_{Al} - 2{}^0G^{hcp}_{Zn}$	15000.00				this work
${}^0G^{Laves-C14}_{Mg:Zn} - {}^0G^{hcp}_{Mg} - 2{}^0G^{hcp}_{Zn}$	−35355.45	8.83886			this work
${}^0L^{Laves-C14}_{Mg,Zn:*}$	8000.00				this work
${}^0L^{Laves-C14}_{*:Mg,Zn}$	35000.00				this work
${}^0L^{Laves-C14}_{Mg,Al:*}$	15000.00				[4]
${}^0L^{Laves-C14}_{*:Mg,Al}$	8000.00				[4]
${}^0L^{Laves-C14}_{*:Al,Zn}$	−7500.00	−18.00000			this work
Mg_2Zn_3; compound energy formalism, $Mg_2(Zn,Al)_3$					
${}^0G^{Mg_2Zn_3}_{Mg:Zn} - 2{}^0G^{hcp}_{Mg} - 3{}^0G^{hcp}_{Zn}$	−54406.20	13.60156			this work
${}^0G^{Mg_2Zn_3}_{Mg:Al} - 2{}^0G^{hcp}_{Mg} - 3{}^0G^{fcc}_{Al}$	1000.00	−0.20000			this work

Table 7
(*Continued*)

MgZn; compound energy formalism, $Mg_{12}(Zn,Al)_{13}$			
${}^0G^{Mg_{12}Zn_{13}}_{Mg:Zn} - 12{}^0G^{hcp}_{Mg} - 13{}^0G^{hcp}_{Zn}$	−236980.84	59.24524	this work
${}^0G^{Mg_{12}Zn_{13}}_{Mg:Al} - 12{}^0G^{hcp}_{Mg} - 13{}^0G^{fcc}_{Al}$	−10000.00	2.50000	this work
Mg_7Zn_3; stoichiometric, $Mg_{51}Zn_{20}$			
${}^0G^{Mg_7Zn_3}_{Mg:Zn} - 51{}^0G^{hcp}_{Mg} - 20{}^0G^{hcp}_{Zn}$	−335741.54	35.50000	this work
Φ-phase; compound energy formalism, $Mg_6(Al,Zn)_5$			
${}^0G^{\Phi}_{Mg:Al} - 6{}^0G^{hcp}_{Mg} - 5{}^0G^{fcc}_{Al}$	−15400.00	−16.50	this work
${}^0G^{\Phi}_{Mg:Zn} - 6{}^0G^{hcp}_{Mg} - 5{}^0G^{hcp}_{Zn}$	−79530.00	20.90	this work
${}^0L^{\Phi}_{Mg:Al,Zn}$	−23100.00	11.00	this work
τ-phase; compound energy formalism, $Mg_{26}(Mg,Al)_6(Al,Mg,Zn)_{48}Al_1$			
${}^0G^{\tau}_{Mg:Mg:Al:Al} - 49{}^0G^{fcc}_{Al} - 32{}^0G^{hcp}_{Mg}$	−81000.00	−186.30	this work
${}^0G^{\tau}_{Mg:Mg:Zn:Al} - {}^0G^{fcc}_{Al} - 32{}^0G^{hcp}_{Mg} - 48{}^0G^{hcp}_{Zn}$	−811620.00	162.00	this work
${}^0G^{\tau}_{Mg:Mg:Mg:Al} - {}^0G^{fcc}_{Al} - 80{}^0G^{hcp}_{Mg}$	405000.00	243.00	this work
${}^0G^{\tau}_{Mg:Al:Al:Al} - 55{}^0G^{fcc}_{Al} - 26{}^0G^{hcp}_{Mg}$	0.00	−105.30	this work
${}^0G^{\tau}_{Mg:Al:Zn:Al} - 7{}^0G^{fcc}_{Al} - 26{}^0G^{hcp}_{Mg} - 48{}^0G^{hcp}_{Zn}$	−832680.00	162.00	this work
${}^0G^{\tau}_{Mg:Al:Mg:Al} - 7{}^0G^{fcc}_{Al} - 74{}^0G^{hcp}_{Mg}$	1053000.00	405.00	this work
${}^0L^{\tau}_{Mg:Mg:Al,Zn:Al}$	−105300.00	243.00	this work
${}^0L^{\tau}_{Mg:Mg:Al,Mg:Al} = {}^0L^{\tau}_{Mg:Al:Al,Mg:Al}$	−202500.00	−40.50	this work
${}^0L^{\tau}_{Mg:Mg:Mg,Zn:Al} = {}^0L^{\tau}_{Mg:Al:Mg,Zn:Al}$	243000.00	81.00	this work
${}^0L^{\tau}_{Mg:Al:Al,Zn:Al}$	−16200.00	243.00	this work

Here ∗ stands for all possible occupations of one of the elements Al, Mg and Zn on the corresponding sublattice.

vious step now was repeated taking into account the parameter ${}^0L^{\tau}_{Mg:Mg:Al,Zn:Al}$. After a few ''trial and error'' iterations these four parameters were adjusted to the mentioned experimental data. Now the parameter ${}^0G^{\tau}_{Mg:Mg:Mg:Al} - {}^0G^{fcc}_{Al} - 80{}^0G^{hcp}_{Mg}$ was set to an arbitrary positive value of $5000+3T$ J/(mol of atoms) and the two interaction parameters ${}^0L^{\tau}_{Mg:Mg:Al,Mg:Al}$ and ${}^0L^{\tau}_{Mg:Mg:Mg,Zn:Al}$ were adjusted to fit the Mg-rich boundary of τ at 608 K. Finally the two parameters ${}^0G^{\tau}_{Mg:Al:Al:Al} - 55{}^0G^{fcc}_{Al} - 26{}^0G^{hcp}_{Mg}$ and ${}^0G^{\tau}_{Mg:Al:Zn:Al} - 7{}^0G^{fcc}_{Al} - 26{}^0G^{hcp}_{Mg} - 48{}^0G^{hcp}_{Zn}$ were adjusted to fit the Mg-poor boundary of τ. During this step the previously adjusted parameters of τ had to be refined again.

Finally the interaction parameter ${}^0L^{\tau}_{Mg:Al:Al,Zn:Al}$ was changed independently of ${}^0L^{\tau}_{Mg:Mg:Al,Zn:Al}$ to adjust the curvature of the Mg-poor boundary of τ independently of that of the Mg-rich one. The temperature dependence of all the later adjusted τ parameters was estimated to get a reasonable Gibbs energy description for τ also at 273 K.

4.3.3.3. β- and γ-Al–Mg phases. After adjusting all τ parameters the ternary parameters of the β and γ-Al–Mg phases mentioned in the previous section were adjusted to fit the Zn-solubilities of these phases. By this treatment the parameter ${}^0G^{\gamma-Al-Mg}_{Mg:Mg:Zn} - 34{}^0G^{hcp}_{Mg} - 24{}^0G^{hcp}_{Zn}$ became negative and predicted stability of this phase in a Zn-rich area. To correct this, a negative interaction parameter ${}^0L^{\gamma-Al-Mg}_{Mg:Mg,Zn:*} = -4000 + 2T$ J/(mol of atoms) was arbitrarily introduced and the parameters adjusted again.

4.3.3.4. Φ-phase:. The three parameters of Φ mentioned in the previous section were adjusted similarly as described for the first three parameters of τ to fit the extension of the homogeneity range in

Table 8
Invariant reactions in the Al–Mg–Zn ternary system

Reaction Type	Temperature [K]			Phase	Calculated Composition (at.%)		
	[9]	this work exp.	this work calc.		Al	Mg	Zn
$L + MgZn_2 \rightleftharpoons \tau$	808	800	803.35	L	21.79	37.14	41.07
Maximum				$MgZn_2$	7.15	33.43	59.42
				τ	18.22	36.24	45.54
$L \rightleftharpoons (Al) + \tau$	762	756	752.84	L	51.19	21.48	27.33
Maximum				(Al)	90.19	4.22	5.59
				τ	23.29	33.82	42.89
$L + \tau \rightleftharpoons (Al) + MgZn_2$	748	752	749.56	L	45.53	18.90	35.57
Transition				(Al)	89.63	3.01	7.36
				$MgZn_2$	7.88	33.12	59.00
				τ	19.75	33.02	47.23
$L \rightleftharpoons \beta + \tau$	722		724.40	L	55.52	39.09	5.39
Maximum				β	56.67	38.86	4.47
				τ	48.02	41.00	10.98
$L \rightleftharpoons \gamma + \tau$	723		724.14	L	46.21	47.24	6.55
Maximum				γ	46.34	49.14	4.52
				τ	45.86	42.39	11.75
$L \rightleftharpoons \beta + (Al)$			723.89	L	63.26	35.74	1.00
Maximum				β	60.01	38.86	1.13
				(Al)	84.00	15.81	0.19
$L \rightleftharpoons \beta + \gamma$			723.35	L	55.67	42.61	1.72
Maximum				β	59.40	38.86	1.74
				γ	50.70	47.57	1.70
$L \rightleftharpoons \beta + \gamma + \tau$	721		721.64	L	51.99	43.14	4.87
Eutectic				β	57.08	38.86	4.06
				γ	49.01	47.07	3.92
				τ	48.62	41.89	9.49
$L \rightleftharpoons \beta + (Al) + \tau$	720		720.24	L	60.13	34.30	5.56
Eutectic				β	56.43	38.86	4.71
				(Al)	85.73	13.26	1.01
				τ	47.68	40.10	12.22
$L + MgZn_2 + \tau \rightleftharpoons Mg_2Zn_3$			706.79	L	5.56	60.63	33.81
Peritectic				$MgZn_2$	3.66	33.82	62.52
				τ	10.73	40.28	48.99
				Mg_2Zn_3	5.00	40.00	55.00
$L + \gamma + \tau \rightleftharpoons \Phi$	666	663	660.52	L	17.27	65.89	16.83
Peritectic				γ	34.05	58.14	7.81
				Φ	26.29	54.54	19.17
				τ	30.03	44.05	25.92
$L + \gamma \rightleftharpoons (Mg) + \Phi$	635	633	639.33	L	13.72	69.79	16.48
Transition				γ	31.98	60.09	7.93
				(Mg)	5.89	92.32	1.79
				Φ	25.67	54.54	19.79
$L + MgZn_2 \rightleftharpoons (Al) + Mg_2Zn_{11}$	638		630.27	L	11.13	7.63	81.24
Transition				(Al)	45.95	0.27	53.78
				$MgZn_2$	2.37	32.75	64.88
				Mg_2Zn_{11}	3.62	15.38	81.00
$L + Mg_2Zn_3 + \tau \rightleftharpoons MgZn$			626.50	L	4.62	68.61	26.77

Table 8
(*Continued*)

Peritectic			Mg_2Zn_3	5.25	40.00	54.75
			τ	12.22	41.69	46.09
			MgZn	5.28	48.00	46.72
$L \rightleftharpoons (Al) + (Zn) + Mg_2Zn_{11}$	616	617.15	L	8.69	5.93	85.38
Eutectic			(Al)	34.78	0.14	65.08
			(Zn)	2.53	0.23	97.24
			Mg_2Zn_{11}	2.80	15.38	81.82
$L + Mg_7Zn_3 \rightleftharpoons (Mg) + MgZn$	612	613.62	L	0.10	70.99	28.91
Transition			(Mg)	0.05	97.00	2.95
			Mg_7Zn_3	0.00	71.83	28.17
			MgZn	0.15	48.00	51.85
$L + \Phi \rightleftharpoons (Mg) + \tau$	616	612.84	L	5.66	69.94	24.40
Transition			Φ	17.41	54.55	28.04
			(Mg)	2.62	94.85	2.53
			τ	15.25	42.34	42.41
$L \rightleftharpoons (Mg) + MgZn + \tau$	611	611.23	L	5.11	69.95	24.94
Eutectic			(Mg)	2.38	95.04	2.58
			MgZn	6.11	48.00	45.89
			τ	14.10	42.17	43.72
$(Al\text{-}1) + MgZn_2 \rightleftharpoons (Al\text{-}2) + Mg_2Zn_{11}$		606.75	(Al-1)	53.17	0.20	46.63
Transition			$MgZn_2$	2.13	32.86	65.01
			(Al-2)	75.87	0.15	23.98
			Mg_2Zn_{11}	3.34	15.38	81.28
$(Mg)+\tau \rightleftharpoons MgZn+\Phi$		598.99	(Mg)	2.35	95.25	2.40
Transition			τ	14.61	42.11	43.28
			MgZn	6.30	48.00	45.70
			Φ	17.05	54.54	28.41
$(Al-1) + Mg_2Zn_{11} \rightleftharpoons (Al-2) + (Zn)$		550.48	(Al-1)	40.99	0.06	58.95
Transition			(Zn)	1.61	0.09	98.30
			(Al-2)	85.82	0.03	14.15
			Mg_2Zn_{11}	2.17	15.38	82.45
$MgZn+\tau \rightleftharpoons Mg_2Zn_3+\Phi$		496.36	MgZn	6.48	48.00	45.52
Transition			τ	16.32	40.72	42.96
			Mg_2Zn_3	6.17	40.00	53.83
			Φ	19.15	54.55	26.30

Al–Zn direction and the temperature of the ternary peritectic formation of Φ.

4.3.3.5. Binary Mg–Zn phases:. In a last step the parameters ${}^0G_{Mg:Al} - q^0G^{fcc}_{Al} - p^0G^{hcp}_{Mg}$ had to be adjusted to the Al solubilities of the binary Mg_pZn_q phases MgZn, Mg_2Zn_3 and Mg_2Zn_{11}.

During all these steps some of the previously adjusted parameters of solid phases had to be refined by small corrections.

4.3.4. Results and calculations

The resulting thermodynamic parameter set of the Al–Mg–Zn ternary system is given in Table 7.

The presented thermodynamic description of the Al–Mg–Zn system is in accordance with most of the experimental information on this system. In Table 8 the calculated and experimental temperatures of invariant equilibria are compared.

The calculated ternary phase diagram is represented by an isothermal section at 608 K in Fig. 5 together with experimental data, by the liquidus surface in Fig. 6, by the (Al)-solvus surface in Fig. 7 and by the (Mg)-solidus and -solvus in Fig. 8.

The calculated vertical sections at 36 at.% Mg, 20 at.% Al and 20 at.% Zn are shown in Figs. 9–11 in comparison with the experimental data mentioned in Section 3 and from literature (the literature data in the

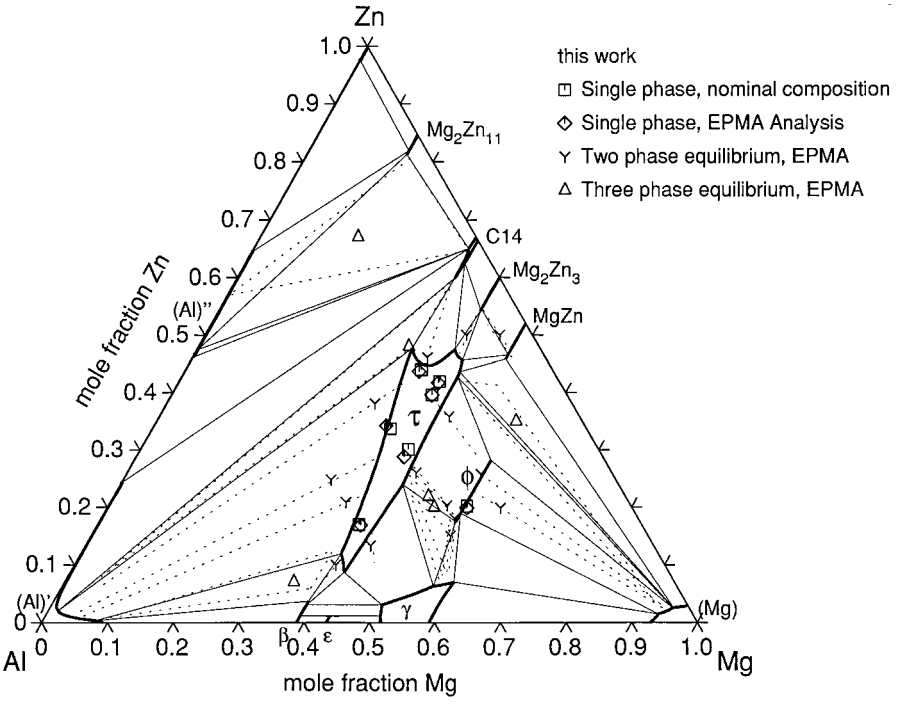

Fig. 5. Isothermal section at 608 K of the Al–Mg–Zn system.

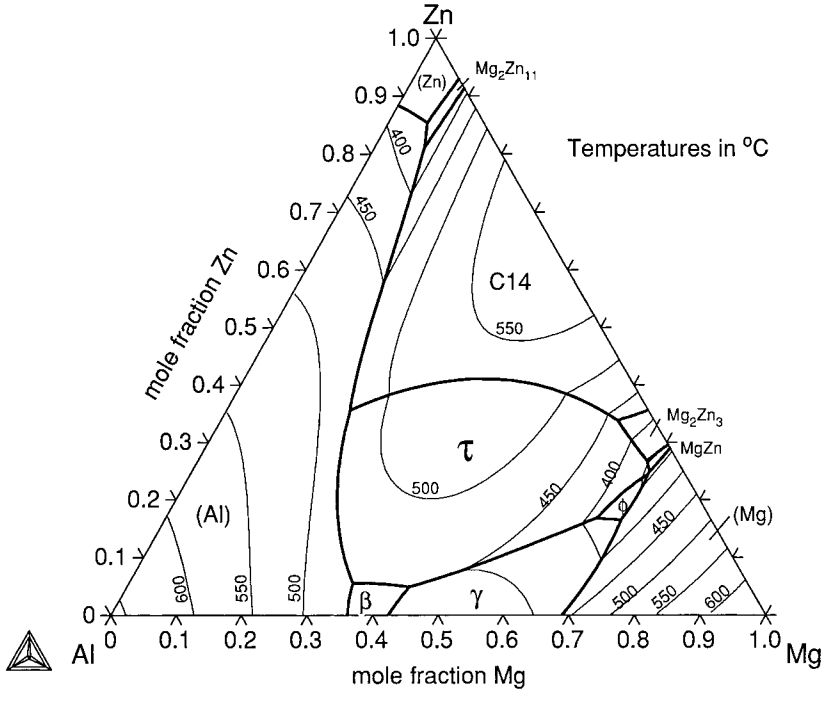

Fig. 6. Liquidus surface of the Al–Mg–Zn system.

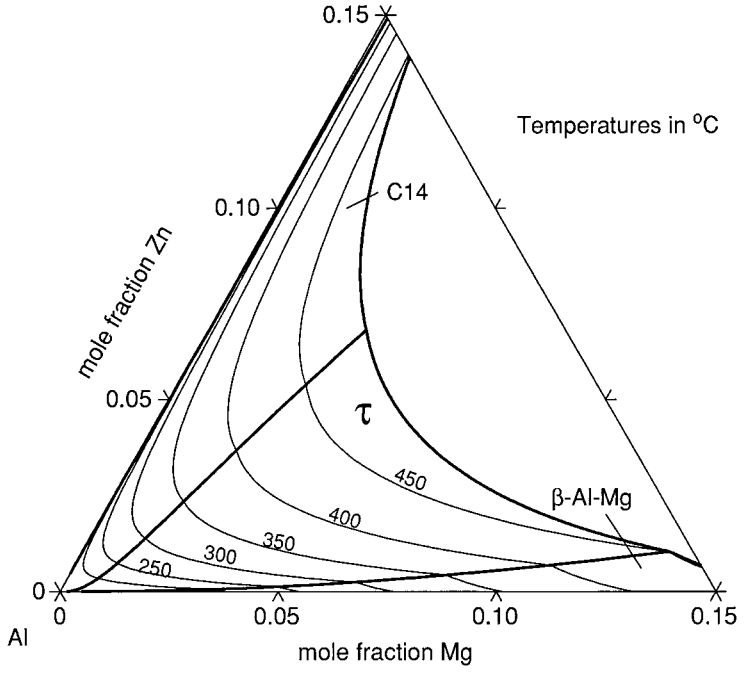

Fig. 7. Solvus of the (Al) solid solutions of the Al–Mg–Zn system.

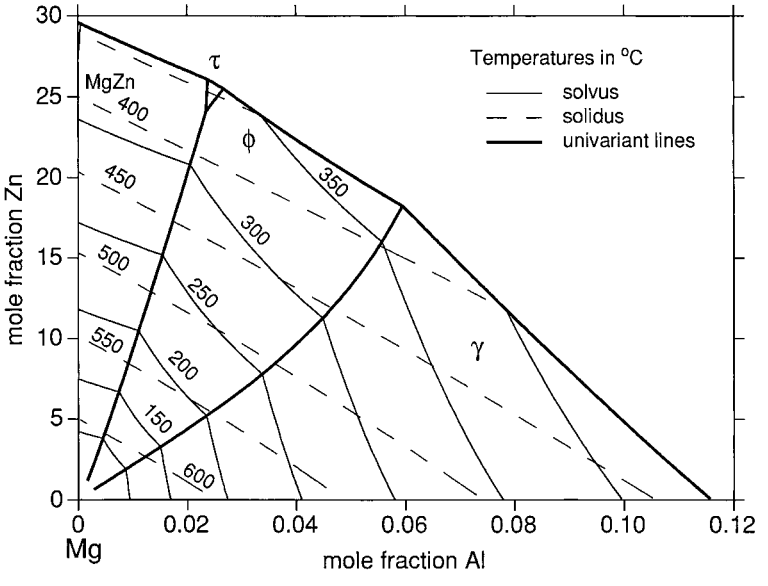

Fig. 8. Solvus and solidus of the (Mg) solid solutions of the Al–Mg–Zn system.

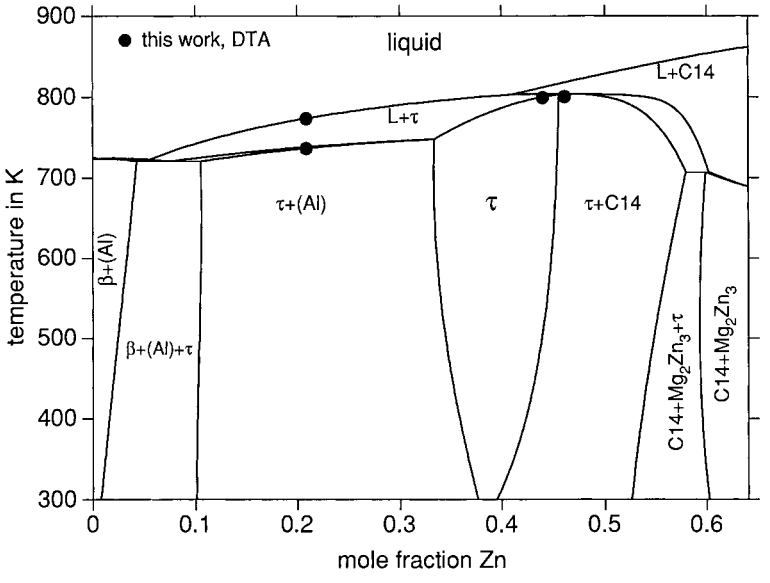

Fig. 9. Vertical section of the Al–Mg–Zn system at 36 at.% Mg.

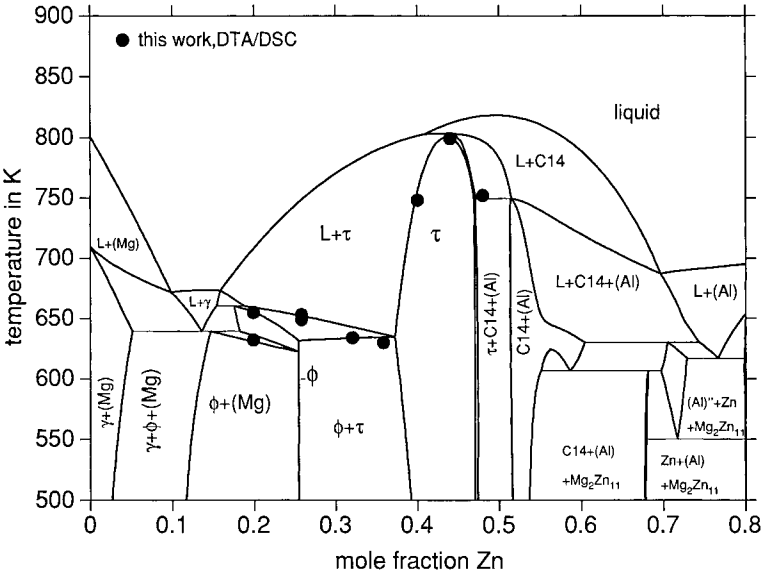

Fig. 10. Vertical section of the Al–Mg–Zn system at 20 at.% Al.

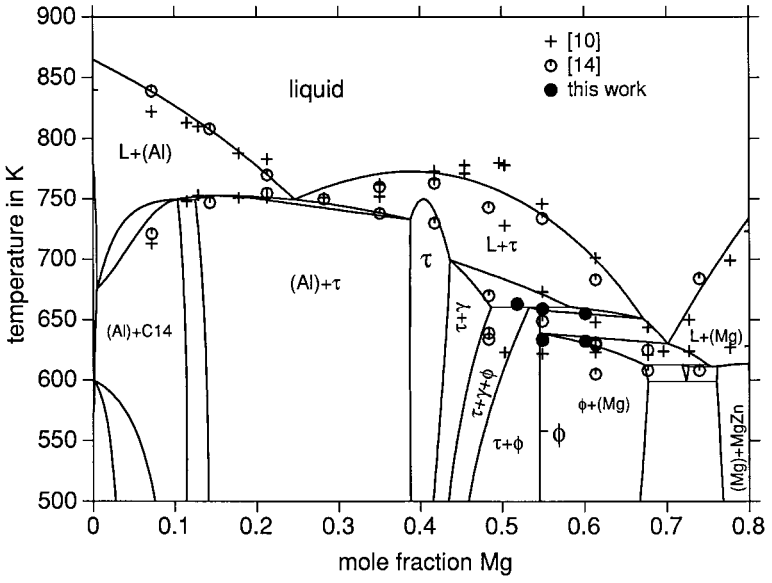

Fig. 11. Vertical section of the Al–Mg–Zn system at 20 at.% Zn.

last figure are for 40 mass% Zn, which nearly coincides with 20 at.% Zn).

5. Conclusion

A consistent set of thermodynamic functions of state for all stable phases existing in the Al–Mg–Zn ternary system was obtained. The calculated phase diagram and the thermodynamic properties agree very well with the experimental data. Thus a reliable basis for evaluation into higher order systems containing the Al–Mg–Zn system as a boundary, has been established, for example into the quaternary Al–Cu–Mg–Zn system.

Acknowledgements

Financial support by the German ''Bundesministerium für Bildung, Wissenschaft, For schung und Technologie'' (Contract 03K7208 0), project COST 507 as well as the European Commission (Human Capital and Mobility, Contract ERBCHRX-CT93-0285, MSIT trainer Network) is gratefully acknowledged.

References

[1] I. Ansara (Ed.), COST 507, Thermochemical database for light metal alloys, Action on Materials Sciences, European Commission, DG XII, Science Research and Development, L-2920 Luxembourg, 1995.
[2] N. Saunders, CALPHAD 14 (1990) 61.
[3] R. Agarwal, S.G. Fries, H.L. Lukas, G. Petzow, F. Sommer, T.G. Chart, G. Effenberg, Z. Metallkd. 83 (1992) 216.
[4] T. Buhler, S.G. Fries, P.J. Spencer, H.L. Lukas, J. Chim. Phys. 94 (1997) 1043.
[5] P. Liang, H.L. Lukas, H.J. Seifert, F. Aldinger, Proceedings of Thermodynamics of Alloys, Marseille, 1996.
[6] I. Hurtado, private communication.
[7] L.D. Willey, Metals Handbook, American Society for Metals, Metals Park, Ohio, vol. 8, 1973, p. 397.
[8] N.U. Despande, K.K. Ray, A.K. Mallik, J. Alloy Phase Diagrams 2 (1986) 108.
[9] D.A. Petrov, in: G. Petzow, G. Effenberg (Eds.), Ternary Alloys, Vol. 7, VCH Verlag, Weinheim, Germany, 1993, p. 57.
[10] G. Eger, Z. Metallkd. 4 (1913) 29.
[11] F. Laves, K. Löhberg, H. Witte, Metallwirtschaft 14 (1935) 793.
[12] G. Bergman, J.L.T. Waugh, L. Pauling, Nature 169 (1952) 1057.
[13] G. Bergman, J.L.T. Waugh, L. Pauling, Acta Crystallogr. 10 (1957) 254.
[14] M. Hamasumi, Sci. Rep. Tôhoku Imp. Univ., 1936 [i], Honda Anniv., Vol. 748.

[15] W. Köster, W. Wolf, Z. Metallkd. 28 (1936) 155.
[16] W. Köster, W. Dullenkopf, Z. Metallkd. 28 (1936) 309.
[17] W. Köster, W. Dullenkopf, Z. Metallkd. 28 (1936) 363.
[18] K. Riederer, Z. Metallkd. 28 (1936) 312–317.
[19] V.I. Mikheeva, O.N. Kryukova, Izv. Akad. Nauk SSSR, Otd. Khim. Nauk 4 (1944) 296.
[20] P.Y. Saldau, Izv. Sekt. Fiz. Khim. Anal. 19 (1949) 487.
[21] J.B. Clark, Trans. Am. Soc. Met. 53 (1961) 295.
[22] P. Donnadieu, A. Quivy, T. Tarfa, P. Ochin, A. Dezellus, M. Harmelin, P. Liang, H.L. Lukas, H.J. Seifert, F. Aldinger, G. Effenberg, Z. Metallkd. 88 (1997) 911.
[23] W.A. Cassada, Y. Shen, S.J. Poon, G.F. Shiflet, Phys. Rev. B 34 (1986) 7413.
[24] T. Rajasekharan, D.A. Akhtar, R. Copalan, K. Muraledharan, Nature 322 (1986) 528.
[25] T. Takcuchi, S. Murasaki, A. Mastumuro, U. Mizutani, J. Non-Cryst. Solids 156–158 (1993) 914.
[26] W. Sander, Z. Anorg. Chem. 154 (1926) 144.
[27] G.G. Urazov, N.A. Filin, A.B. Shashin, Metallurgy (The Metallurgist) 15 (1940) 3.
[28] E. Butchers, G.V. Raynor, W. Hume-Rothery, J. Inst. Met. 69 (1943) 209.
[29] E. Butchers, W. Hume-Rothery, J. Inst. Met. 71 (1945) 291.
[30] V.I. Mikheeva, O.N. Kryukova, Dokl. Akad. Nauk. SSSR 50 (1945) 243.
[31] I.A. Aleksakhin, A.A. Semionow, Metalloved. Term. Obrab. Met. 4 (1962) 40; Metal Science and Heat treatment of Metals, (1962) 160 (English).
[32] G.M. Kuznetsov, A.D. Barsukov, G.B. Krivosheeva, V.A. Istomin-Kastrovskii, Izv. Vyss. Uchebn. Zaved. Tsvetn. Metall. No. 1, (1985) 88; Soviet Non-Ferrous Metals Research 1 (1985) 65 (English).
[33] L.F. Mondolfo, Met. Reviews 16 (1971) 95.
[34] L.F. Mondolfo, Aluminium Alloys; Structure and Properties, Butterworths, 1976, p. 575.
[35] H. Haneman, A. Schrader, Ternary Al Alloys, Atlas Metallographicus, Verlag Stahleisen M.B.H. Düsseldorf, Vol. 3, Part 2, 1952, p. 133.
[36] W. Stiller, H. Hoffmeister, Z. Metallkd. 70 (1979) 817.
[37] G.M. Kuznetsov, A.D. Barsukov, G.B. Krivosheeva, E.V. Bashashkina, Izv. Vyss. Uchebn. Zaved. Tsvetn. Metall., vol. 2, 1985, 91.
[38] A.A. Bochvar, M.O. Kuznetzov, Metallurgy (The Metallurgist) 8 (1933) 7.
[39] P. Saldau, M. Zamotorin, Z. Anorg. Chem. 213 (1933) 377.
[40] P. Saldau, M. Zamotorin, Izv. Sekt. Fiz. Khim. Anal. 11 (1938) 27.
[41] A.T. Little, G.V. Raynor, W. Hume-Rothery, J. Inst. Met. 69 (1943) 423.
[42] A.T. Little, G.V. Raynor, W. Hume-Rothery, J. Inst. Met. 69 (1943) 467.
[43] G. Siebel, Z. Elektrochem. 49 (1943) 218.
[44] D.J. Strawbridge, W. Hume-Rothery, A.T. Little, J. Inst. Met. 74 (1948) 191.
[45] M.I. Zamotorin, Trudy Leningrad. Politekhn. Inst. 180 (1955) 38.
[46] P. Saldau, State Publishing House (Defence), Moscow, 1961, 5.
[47] V.I. Mikheeva, O.N. Kryukova, Dokl. Akad. Nauk. SSSR 50 (1945) 247.
[48] W.L. Fink, L.A. Willey, Metals Tech., Techn. Publ. N° 761, 3(8) (1936) 1.
[49] W.L. Fink, L.A. Willey, Trans. Met. Soc. AIME 124 (1937) 78.
[50] J.B. Clark, F.N. Rhines, Trans. Am. Soc. Met. 51 (1959) 199.
[51] Z. Kozuka, J. Moriyama, I. Kushima, J. Electrochem. Soc. Jpn. 28 (1960) 298.
[52] E.E. Lukashenko, A.M. Pogodaev, Russ. J. Phys. Chem. 45 (1971) 1182.
[53] A.M. Pogodaev, E.E. Lukashenko, Russ. Metall. 6 (1974) 74.
[54] Y.B. Kim, F. Sommer, B. Predel, J. Alloys Comp. 247 (1997) 43.
[55] S.-L. Chen, Ph.D. Thesis, University of Wisconsin-Madison, Madison, WI, 1994.
[56] H.L. Su, M. Harmelin, P. Donnadieu, C. Bätzner, H.J. Seifert, H.L. Lukas, G. Effenberg, F. Aldinger, J. Alloys Comp. 247 (1997) 57.
[57] T. Gödecke, F. Sommer, private communication.
[58] M. Hansen, K. Anderko, Constitution of Binary Alloys, McGraw-Hill, New York, 1958.
[59] T.B. Massalski (Ed.), Binary Alloy Phase Diagrams, ASM, Metals Park, Ohio, 1990.
[60] P. Chartrand, A.D. Pelton, J. Phase Equilibria 15 (1994) 591.
[61] E. Schürmann, E. Voss, Giessereiforschung 33 (1981) 43.
[62] P. Donnadieu, H.L. Su, A. Proult, M. Harmelin, G. Effenberg, F. Aldinger, J. Phys. I France 6 (1996) 1153.
[63] P. Donnadieu, M. Harmelin, H.J. Seifert, F. Aldinger, Phil. Mag. B., to be submitted.
[64] I. Ansara, T.G. Chart, A. Fernández Guillermet, F.H. Hayes, U.R. Kattner, D.G. Pettifor, N. Saunders, K. Zeng, CALPHAD 21 (1997) 171.
[65] M. Kowalski, P.J. Spencer, J. Phase Equilibria 14 (1993) 432.
[66] J.G. Costa Neto, S.G.- Fries, H.L. Lukas, CALPHAD 17 (1993) 219.
[67] G.C. Coelho, S.G. Fries, H.L. Lukas, P. Majewski, J.M. Zelaya Bejarano, S. Gama, C. A. Ribeiro, G. Effenberg, Klaus schulze, symposium on processing and applications of high purity refractory metals and alloys, in: P. Kumar, H.A. Jehn, M. Uz (Eds.), The Minerals, Metals and Materials Society, Warrendale, PA, 15086, USA, 1994.
[68] A.T. Dinsdale, CALPHAD 15 (1991) 319.
[69] S. an Mey, Z. Metallkd. 84 (1993) 451.